# Journal of Materials Chemistry B

Accepted Manuscript

This article can be cited before page numbers have been issued, to do this please use: P. Singh, L. S. Mittal, V. vanita, K. Kumar, A. Walia, G. Bhargava and S. kumar, *J. Mater. Chem. B*, 2016, DOI: 10.1039/C6TB00512H.




ROYAL SOCIETY OF CHEMISTRY

www.rsc.org/materialsB

View Article Online
DOI: 10.1039/C6TB00512H

# Self-assembled vesicle and rod-like aggregates of functionalized perylene diimide: Reaction based near-IR intracellular fluorescent probe for selective detection of palladium

Prabhpreet Singh,*[a] Lalit Singh Mittal,[a] Vanita Vanita,[b] Kapil Kumar,[a] Amandeep Walia,[b] Gaurav Bhargava,[c] Subodh Kumar[a]

[a]*Department of Chemistry, UGC Centre for Advanced Studies, Guru Nanak Dev University, Amritsar 143 005, India.*

*e-mail: prabhpreet.chem@gndu.ac.in; Tel: +91-84271-01534bb*

[b]*Department of Human Genetics, Guru Nanak Dev University, Amritsar 143 005, India.*

[c]*Department of Applied Sciences, Punjab Technical University, Kapurthala-144601, Punjab, India.*

Nanovesicle and rod-like aggregates of **PS-PDI** after $Pd^0$ based depropargylation shows de-aggregation and near-infrared, ratiometric absorbance and emission changes in water, drug, environmental samples and live HeLa cells.

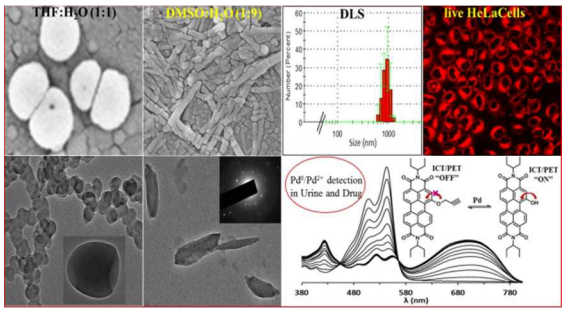

View Article Online
DOI: 10.1039/C6TB00512H

Journal Name

ARTICLE

# Self-assembled vesicle and rod-like aggregates of functionalized perylene diimide: Reaction based near-IR intracellular fluorescent probe for selective detection of palladium

Received 00th January 20xx,
Accepted 00th January 20xx

DOI: 10.1039/x0xx00000x

www.rsc.org/

Prabhpreet Singh,*[a] Lalit Singh Mittal,[a] Vanita Vanita,[b] Kapil Kumar,[a] Amandeep Walia,[b] Gaurav Bhargava,[c] Subodh Kumar[a]

**Abstract**: Herein, we report design, synthesis and self-assembly of perylenediimide (PDI) based near-IR intracellular probe (**PS-PDI**). **PS-PDI** molecules undergo aggregation to form self-assembled nanospheres and nanorods morphology in THF:$H_2O$ (1:1) and DMSO:$H_2O$ (1:9), respectively. The nanospheres have an open hole on surface reminiscent of vesicle structure (with diameter of internal void in the range of 20-25 nm) whereas length of the nanorods extended up to few µm range. The $Pd^0$ based depropargylation leads to de-aggregation of these **PS-PDI** aggregates into smaller spherical aggregates as evidenced by DLS, SEM and TEM studies. Interestingly, these aggregates of **PS-PDI** in solution show highly sensitive behavior in the presence of $Pd^0$ showing absorbance changes in NIR region ($\lambda_{max}$ = 710 nm) and quenching of emission at $\lambda_{em}$ 630 nm (DMSO:$H_2O$, 1:9) with limit of detection = 6.6 x $10^{-9}$ M or at $\lambda_{em}$ 564 nm (THF:$H_2O$, 1:1) with limit of detection = 2.1 x $10^{-8}$ M. Time and concentration dependent kinetics profiles of **PS-PDI** aggregates revealed impressive rate constant value of 0.4 $s^{-1}$ and 0.21 $s^{-1}$ (DMSO:$H_2O$, 1:9), respectively in fluorescence and UV-Vis spectroscopy using 2x$10^{-5}$ M concentration of $Pd^0$. **PS-PDI** undergoes rapid internalization into HeLa cells with low cytotoxicity and successfully used as intracellular imaging reagent for $Pd^0$ in live HeLa cell. For practical application, we have exploited these nano-aggregates of **PS-PDI** for estimation of $Pd^{2+}$ in the presence of $NaBH_4$-$PPh_3$ mixture, $Pd^0$ in drug and environmental samples and $Pd^{2+}$ in urine sample with excellent selectivity and sensitivity.

## 1. Introduction

Perylenediimides (PDIs) are well documented class of functional organic dyes with excellent electronic, optical and redox properties.[1-5] Due to these properties PDIs may find applications in dyes and pigments industries,[6] optoelectronic devices[7-9] and supramolecular chemistry.[10-20] The aggregation and optoelectronic properties of PDIs can be tailored through modification of its π-molecular structure with chemical groups[1,21-22] either or both at the imide or bay positions of the PDIs core. Due to presence of planar π-conjugated core, PDI has propensity for aggregation in aqueous medium via π-π stacking, hydrogen bonding, electrostatic and solvation interactions. Although many reports regarding modification of imide position of PDIs to generate self-assembled nanostructures are being published each year[23-24] however, little attention has been paid to the self-assembly of bay substituted PDIs.[25-26] Probably, the substitutions at bay position drastically increase the solubility of PDIs and if substituents are bulky in nature, the perylene backbone deviate from planarity to minimize the strain and this hinders the possibility of π-π stacking. Moreover, the application of self-assembled PDIs for molecular recognition of metal ions and anions in water via aggregation or de-aggregation of PDIs has been scarcely reported due to the poor solubility of PDIs in aqueous medium. Earlier we have reported (ionic)self-assembly of benzimidazolium, amino acids and nucleobase-functionalized carbon nanotubes (CNTs)[27-29] and now we envisage that ease in aggregation of perylene chromophore in aqueous medium could be exploited for molecular recognition by using stimuli based aggregation-disaggregation of PDIs. In this context, we recently synthesized PDI based probe and

[a] Department of Chemistry, UGC Centre for Advanced Studies, Guru Nanak Dev University, Amritsar 143 005, India
email: prabhpreet.chem@gndu.ac.in; Tel: +91-84271-01534
[b] Department of Human Genetics, Guru Nanak Dev Univerity, Amritsar 143 005, India
[c] Department of Applied Sciences, IK Gujral Punjab Technical University, Kapurthala-144601, Punjab, India

† Footnotes relating to the title and/or authors should appear here.
Electronic Supplementary Information (ESI) available: [Structural data, self-assembly, spectroscopic and photophysical data of **PS-PDI** and control molecules with additional information]. See DOI: 10.1039/x0xx00000x

View Article Online
DOI: 10.1039/C6TB00512H





judiciously utilized its aggregation behavior for detection of perchlorate anion in water and C6 glioma cells.[10]

Palladium is well known for its role as catalyst in organic synthesis (drugs) and thus extensively used in pharmaceutical industry.[30] Palladium is also widely used in several materials such as jewellery, automobiles, dental crowns and fuel cells. Palladium species can also interact and form complexes with biomolecules and may interfere with cellular processes.[31] Thus, our environment is continuously being polluted with Palladium that poses serious human and environmental health hazards. Several conventional analytical methods have been developed to detect palladium species,[32] however ratiometric chromo-fluorescent probes with a convenient operation design principal provide an edge over these methods in terms of naked eye visibilty, low cost, sensitivity and selectivity.[33] Moreover probes showing absorption and emission maxima at >600 nm could be beneficial for cellular applications.

Chemodosimeter, as defined by Chae and Czarnik, is an abiotic molecule which shows irreversible transduction of an observable signal on analyte recognition.[34] Depropargylation / deallylation[35] of propargyloxy and allyloxy derivatives of fluorophores and chromophores have provided a general method for the development of $Pd^0$ selective chemodosimeters. PDIs due to their electron deficient nature show large internal charge transfer (ICT) phenomenon in the presence of electron donating groups, but have found limited applications in developing $Pd^0$ probes.[17] We envisaged that if the propargyloxy group on PDI undergoes efficient $Pd^0$ depropargylation, it will result in formation of phenoxide derivatives under physiological conditions and thus would result in enhanced ICT process and is expected to shift the absorption band towards longer wavelength.

In the work reported herein, we have designed new PDI based mono-propargyloxy derivatives **PS-PDI** and PDI **5** having N-(ethylpropyl) and N-cyclohexyl group, respectively at imide positions and bis-propargyloxy derivative **DPS-PDI** substituted with N-(ethylpropyl) group at imide positions. **PS-PDI** transformed into nanospheres with an open hole on the surface in THF:$H_2O$ (1:1), whereas it generates nanorods self-assembly in DMSO:$H_2O$ (1:9).

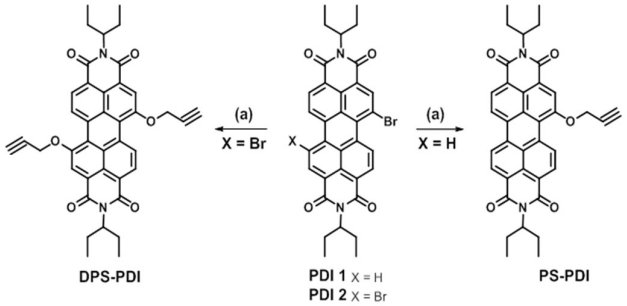


**Scheme 1**. Synthesis of the chemodosimeters **PS-PDI** and **DPS-PDI**; Reagents and conditions (a) propargyl alcohol, $K_2CO_3$, DMF, 90°C, 9h.

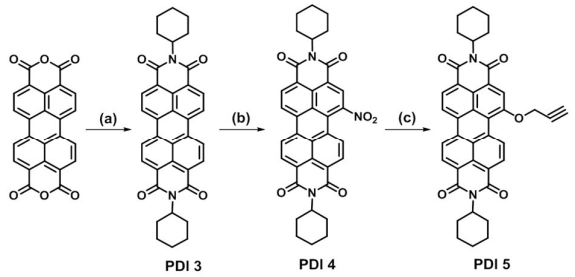


**Scheme 2**. Synthesis of the chemodosimeter PDI **5**; Reagents and conditions (a) cyclohexyl amine, imidazole, 140°C, 4h; (b) ceric ammonium nitrate, $H_2SO_4$-$HNO_3$ mixture, RT, 10 min; (c) propargyl alcohol, $K_2CO_3$, DMF, 80°C, 2h.

On addition of $Pd^0$, the nanovesicles or nanorods assembly disintegrate to form smaller nanospherical structures. Amongst **PS-PDI** and PDI **5**, the former show significantly higher solubility (better than earlier literature report) and shows higher sensitivity towards $Pd^0$ using DMSO:$H_2O$ (1:9, where **PS-PDI** exist in aggregated form) both in absorption and fluorescence spectrum. Bis(propargyloxy) derivatives **DPS-PDI** show equally good solubility in mixed aqueous medium but lesser change in absorption and fluorescence spectrum was observed. The **PS-PDI** has been successfully used for determination of $Pd^0$ in live HeLa cells through confocal imaging.

## 2. Experimental Section

### 2.1 Materials and Characterization

Chemicals and solvents were of reagent grade and used without further purification unless otherwise stated. All reactions were performed under $N_2$ atmosphere. DMF, DMSO, and Tetrahydrofuran (THF) solvents were of HPLC grade. Deionized water was obtained from ULTRA UV/UF Rions Lab Water System Ultra 370 series. Chromatographic purification was done with silica gel 60-120 mesh. TLC was performed on aluminium sheets coated with silica gel 60 F254 (Merck, Darmstadt). PDI **1**[36a], PDI **2**[10] and PDI **3**[36b] were synthesized according to literature procedures. NMR spectra were recorded on Bruker and JEOL (operating at 500 and 400 MHz for $^1H$; 125 and 100 MHz for $^{13}C$, respectively). The peak values were obtained as ppm (δ), and referenced to the TMS as reference in $^1H$ NMR and deutrated solvent in $^{13}C$ NMR spectra. Abbreviations used for splitting patterns are s = singlet, bs = broad singlet, t = triplet, q = quartet, m = multiplet. The absorption spectra were recorded on Shimadzu-2450 spectrophotometer from Shimadzu equipped with Peltier system as temperature controller. Quartz cells of appropriate length were used for sample measurement. The spectral bandwidth and the scan rate were fixed at 2 nm and 140 nm $min^{-1}$, respectively. The fluorescence titrations were

View Article Online
DOI: 10.1039/C6TB00512H




performed on Varian Carey Eclipse fluorescence spectrophotometer using slit width (excitation = 10 nm, emission = 3 nm) with excitation at 500 nm, unless otherwise stated. Fourier transform infrared (FT-IR) spectra were recorded on Perkin Elmer 92035. High resolution mass spectra were recorded on a MALDI ultraflex TOF. Confocal microscopy imaging was carried out with NIKON AIR confocal laser scanning microscope using diode laser excitation at 490 nm. Imaging was performed with Plan Apo 60X objective lens with oil-emersion. Dynamic Light Scattering (DLS) measurements were performed at 25.0 ± 0.1°C using a light-scattering apparatus (Zetasizer Nano ZS Malvern Instrument Ltd., U.K.). SEM measurements were performed on a ZEISS SUPRA$^{TM}$55 operating at an acceleration voltage of 10 KV with tungsten filament as electron source. The TEM images were obtained with a JEOL JEM-2100 electron microscope operating at an acceleration voltage of 200 kV.

#### 2.2 Synthesis of PS-PDI

A mixture of propargyl alcohol (12.8 mg, 13.3 µL, 0.229 mmol) and $K_2CO_3$ (47.3 mg, 0.343 mmol) was stirred in dry DMF (2 mL) under $N_2$ atmosphere. Then, PDI **1** (50 mg, 0.076 mmol) was added and the reaction mixture was stirred at 90$^o$C for 8-9 hours. After cooling to RT, the reaction mixture was poured into ice cold water and the precipitates obtained were filtered. After drying under vacuum, crude **PS-PDI** obtained was further purified by column chromatography ($SiO_2$, Chloroform/ Hexane) to isolate pure **PS-PDI**, red colour solid**;** yield 30 mg (0.051 mmol, 62.2%); $R_f$ = 0.6 (Chloroform/Hexane 9:1). $^1$H NMR (500 MHz, $CDCl_3$, 25 °C): δ 9.56 (d, 1H, *J* = 8.5 Hz, perylene-ArH), 8.68-8.57 (m, 6H, perylene-ArH), 5.23 (d, 2H, *J* = 2.0 Hz, propargyl -$CH_2$), 5.10-5.05 (m, 2H, ethylpropyl), 2.73 (t, *J* = 2.0, 1H, propargyl -CH), 2.30-2.25 (m, 4H, ethylpropyl), 1.99-1.93 (m, 4H, ethylpropyl), 0.96-0.92 (m, 12H, ethylpropyl); $^{13}$C NMR (125 MHz, DMSO-$d_6$): δ 164.6, 156.3, 134.3, 134.0, 133.9, 129.2, 129.0, 128.5, 126.9, 125.0, 123.5, 122.1, 121.7, 77.9, 77.1, 58.0, 57.8, 57.7, 25.2, 11.5; IR (ATR): *v* = 3268, 2965, 2928, 2875, 2121, 1698, 1652, 1591, 1330, 1254, 1065, 908, 747; HRMS: calcd for $C_{37}H_{32}N_2O_5$ (M + $H^+$) 585.23, found 585.776; $\lambda_{abs}$ 543 nm and $\lambda_{em}$ 564 nm (THF).

#### 2.3 Synthesis of DPS-PDI

To a mixture of propargyl alcohol (73.2 mg, 76 µL, 1.30 mmol) and $K_2CO_3$ (270.4 mg, 1.95 mmol) in dry DMF (10 mL) under $N_2$ atmosphere was added PDI 2 (300 mg, 0.435 mmol) at RT. The temperature was raised to 80-90$^o$C and reaction continued for 8-9 hours. After cooling to RT, the reaction mixture was poured into ice cold water and the precipitates obtained were filtered. After drying under vacuum, crude **DPS-PDI** was obtained which was further purified by column chromatography ($SiO_2$, Chloroform/ Hexane) to isolate pure **DPS-PDI,** red colour solid**;** yield 80 mg (0.125 mmol, 30%); $R_f$ = 0.4 (Chloroform/Hexane 9:1). $^1$H NMR (500 MHz, $CDCl_3$, 25 °C): δ 9.56 (d, 2H, *J* = 8.5 Hz, perylene-ArH), 8.60 (d, 2H, *J* = 8.5 perylene-ArH), 8.58 (s, 2H, perylene-ArH), 5.18 (d, 4H, *J* = 2.5 Hz, propargyl-$CH_2$), 5.11-5.04 (m, 2H, ethylpropyl), 2.69 (t, *J* = 2.5, 2H, propargyl -CH), 2.32-2.23 (m, 4H, ethylpropyl), 2.00-1.91 (4H, m, ethylpropyl), 0.94 (t, *J* = 7.5, 12H, ethylpropyl); $^{13}$C NMR (125 MHz, $CDCl_3$): δ 164.3, 155.4, 133.5, 129.8, 129.3, 129.2, 124.5, 123.9, 122.4, 122.1, 122.0, 118.4, 77.6, 77.3, 57.9, 57.8, 25.2, 11.5; IR (ATR): *v* = 3268, 2975, 2875, 2123, 1694, 1658, 1590, 1325, 1232, 1065, 900, 647; HRMS: calcd for $C_{40}H_{34}N_2O_6$ (M + $H^+$) 639.24, found 639.67; $\lambda_{abs}$ 550, 521 nm and $\lambda_{em}$ - 570 nm (THF).

#### 2.4 Synthesis of PDI 4[37a]

The mixture of PDI **3** (2 g, 3.6 mmol), Ceric ammonium nitrate (2.4 g, 4.3 mmol), nitric acid (2.8 mL) and $H_2SO_4$ (5 mL) was stirred in $CHCl_3$ at room temperature for 10 minutes. The reaction mixture was then neutralized with water and organic layer was extracted. The solvent was evaporated under vacuum and crude product was purified by column chromatography ($SiO_2$, chloroform/hexane) to isolate pure PDI **4,** red solid, yield 2.01 gm (3.35 mmol, 93%); $R_f$ = 0.6 (chloroform/hexane 70:30); $^1$H NMR (500 MHz, $CDCl_3$, 25 °C): δ 8.74 (d, 1H, *J* = 8 Hz), 8.69-8.62 (m, 4H), 8.54 (d, 1H, *J* = 8.5 Hz), 8.16 (d, 1H, *J* = 8 Hz), 5.02-5.01 (m, 2H), 2.55-2.53 (m, 4H), 1.94-1.92 (m, 4H), 1.78-1.76 (m, 8H), 1.49-146 (m, 4H); $^{13}$C NMR (125 MHz, $CDCl_3$, 25 °C): δ 163.6, 163.3, 163.2, 162.3, 147.8, 135.5, 133.0, 132.9, 131.4, 131.2, 129.4, 129.3, 129.0, 128.0, 127.5, 126.6, 126.5, 126.4, 125.5, 124.8, 124.5, 124.1, 123.7, 77.4, 54.7, 54.4, 29.3, 29.2, 26.7, 26.6, 25.6, 25.5.

#### 2.5 Synthesis of PDI 5[37b]

The mixture of propargyl alcohol (18.56 mg, 19.3 µL, 0.331 mmol), $K_2CO_3$ (49 mg, 0.363 mmol) and PDI **4** (100 mg, 0.166 mmol) was stirred in DMF at 80$^o$C for 2 h. After completion of the reaction the solvent was removed under vacuum. The reaction mixture was treated with water and was extracted with $CHCl_3$. The crude product was further purified by column chromatography ($SiO_2$, chloroform/hexane) to isolate pure PDI **5,** red solid (0.107 mmol, 65%); $R_f$ = 0.4 (chloroform/ethyl acetate 96:4); $^1$H NMR (500 MHz, $CDCl_3$, 25 °C): δ 9.67 (d, 1H, *J* = 8.5 Hz), 8.77-8.65 (m, 6H), 5.32 (s, 2H), 5.11-5.06 (m, 2H), 2.73 (s, 1H), 2.59-2.52 (m, 4H), 2.01-1.98 (m, 4H), 1.80-1.88 (m, 8H), 1.48-1.55 (m, 4H); $^{13}$C NMR (75 MHz, TFA:$CDCl_3$ (1:9), 25 °C): δ 165.87, 157.44, 135.89, 135.60, 135.28, 133.77, 132.47, 130.92, 130.21, 129.29, 128.71, 127.17, 125.01, 124.91, 124.02, 123.52, 122.96, 122.90, 122.73, 121.82, 120.68, 78.16, 58.02, 56.57, 56.47, 29.50, 29.47, 26.66, 25.47; $\lambda_{abs}$ 550, 521 nm and $\lambda_{em}$ - 570 nm (THF).

## 3. Results and Discussion

#### Synthesis

View Article Online
DOI: 10.1039/C6TB00512H





The bis-propargyloxy substituted perylenediimde **DPS-PDI** was synthesized by aromatic nucleophilic substitution reaction of regio-isomerically pure PDI **2**[10] with propargyl alcohol in DMF (Scheme 1). As far as chemodosimeter principle is concerned we proposed that even mono functionalization of PDI can create desired optical signals in the presence of target analyte. So, the mono-propargyloxy substituted perylenediimde **PS-PDI** was prepared from PDI **1** using the similar protocol as described for **DPS-PDI** (Scheme 1). For the synthesis of PDI **5**, first nitration of PDI **3** has been performed according to modified procedure. Briefly, PDI **3** was treated with ceric ammonium nitrate (CAN), with immediate addition of $H_2SO_4$-$HNO_3$ mixture at room temperature to afford PDI **4** in 10 min in 93% yield. Finally, the reaction between PDI **4** and propargyl alcohol was performed in DMF using $K_2CO_3$ as base to isolate PDI **5** (Scheme 2). The structure of PDI derivatives have been unequivocally proved using NMR ($^1H$, $^{13}C$) spectroscopic analysis, FTIR, ESI-MS and photophysical measurements in solution phase (Fig. S1-S4, ESI).

### Self-assembly and photophysical properties

Although, chemodosimeter **PS-PDI** and PDI **5** seems to be hydrophobic by looking at their structures, the presence of ethylpropyl and cyclohexyl group respectively, at the imide positions and O-propargyl group at the bay position in both chemodosimeters greatly affected their solubility in aqueous medium. So, firstly we studied the effect of organic solvents on the optical properties of **PS-PDI**. The **PS-PDI** shows almost identical absorption maxima (±5 nm) in the different polarity solvents and similarly, no significant change in the emission maxima (±5 nm) were observed. Moreover, no deviation was observed in Frank-Codon factor ($A_{0-0}/A_{0-1}$ = 1.4-1.5)[1] with change in polarity of the solvents which indicates that **PS-PDI** remains in molecularly dissolved state in these solvents (Fig. S5, table S1, ESI).

The optical properties of **PS-PDI** in the mixed organic-aqueous solvents such as THF:$H_2O$ and DMSO:$H_2O$ were also recorded. We observed that upon increasing fraction of water ($f_w$ = 60%, v/v) in THF, **PS-PDI** (1x10$^{-5}$ M) shows the presence of sharp signature peaks around 450-550 nm in the absorption spectrum and intensity remained unperturbed ($A_{0-0}/A_{0-1} \approx 1.4$). However, at $f_w$ = >60%, hypochromic effect on absorption maxima at 543 nm along with broadening of spectrum around 600-750 nm due to Mie scattering was observed (Fig. 1a). The fluorescence spectrum of **PS-PDI** (c = 1x10$^{-5}$ M) in THF showed high emission intensity at 564 nm along with shoulder band at 600 nm. At $f_w$ = 60%, the emission maximum was red-shifted to 570 nm along with hypochromic effect and a shoulder band appeared at 608 nm. Whereas at $f_w$ = 90%, the emission maxima at 570 nm, which corresponds to molecularly dissolved state, disappeared and shoulder band at 608 nm red shifted to 614 nm indicating the aggregation of **PS-PDI** (Fig. S6a, ESI). Although at $f_w$ = 70% or 90% in THF, the aggregation

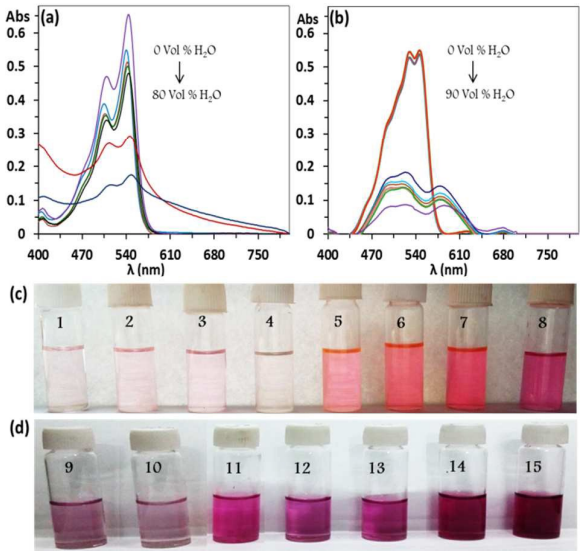


**Fig. 1** UV-Vis absorption changes of **PS-PDI** after incremental addition of $H_2O$ in (a) THF and (b) DMSO at a concentration of 1x10$^{-5}$ M; (c) Photographs showing the solubility of PDI **5** (1-4) and **PS-PDI** (5-8) in aqueous THF mixture; vial no. 1,5 = THF only; 2,6 = T:H (7:3); 3,7 = T:H (5:5); 4,8 = T:H (3:7); (d) Photographs showing the solubility of PDI **5** (9-10) and **PS-PDI** (11-15) in aqueous DMSO mixture; vial no. 9,12 = D:H (5:5); 10,13 = D:H (1:9); 11 = T:H (1:9) for comparison purpose; 14,15 = D:H (1:9) but concentration of **PS-PDI** is 3x10$^{-5}$ and 5x10$^{-5}$ M respectively. All images are at concentration of 1x10$^{-5}$ M unless otherwise stated. T = THF; D = DMSO; H = $H_2O$ in v/v ratio.

has started but visually the **PS-PDI** at 1x10$^{-5}$ M concentration remained soluble (solution stable for more than one week) (Fig. 1c-d, vial no. 5-8 and 11).

Conversely, in solution of DMSO, when $f_w$ = 50%, we observed complete loss of fine structure in the absorption spectrum of **PS-PDI** (c = 1x10$^{-5}$ M). The maxima at 543 nm got blue shifted at 510-520 nm and new broad absorption maxima at 574 nm was observed (Fig. 1b). The emission maxima of **PS-PDI** at 574 nm in DMSO got quenched at $f_w$ = 30-60%, followed by appearance of red shifted emission band at 630 nm ($f_w$ = 70-90%) which indicate the transformation of monomeric PDI molecule to aggregated form due to π-π stacking (Fig. S6b, ESI). Impressively, 1x10$^{-5}$, 3x10$^{-5}$ and 5x10$^{-5}$ M solution of **PS-PDI** in DMSO:$H_2O$ (1:9) remained soluble and stable for at least 3 days without visual precipitation (Fig. 1d, vial no. 12-15).

The absorption spectrum of **DPS-PDI** exhibit fine structure up to 60% $H_2O$:THF and 10% $H_2O$:DMSO mixture, however at $f_w$ = 90% in both cases, we observed blue shifted band at ~506 and ~480 nm. Similarly, **DPS-PDI** shows emission at 574 and 585 nm in 60% $H_2O$:THF and 20% $H_2O$:DMSO mixture, respectively, which got red shifted to 630 nm in 90% $H_2O$:THF or $H_2O$:DMSO mixture (Fig. S7, ESI).

The optical properties of PDI **5** were also recorded in these solvents. However, we observed that PDI **5** has less solubility in comparison to **PS-PDI** (Fig. 1c-d, vial no. 1-4, 9-10). PDI **5** shows absorption maxima at 540 nm in THF or DMSO. At $f_w$ =

View Article Online
DOI: 10.1039/C6TB00512H




60% in THF, the absorption intensity gradually decreased and further addition of water results in precipitation whereas in 10% $H_2O$:DMSO PDI **5** shows fine structure and further increase in water fraction leads to blue shift at 492 nm ($A_{0-0}/A_{0-1}$ = 0.5). The PDI **5** remained emissive up to 50% $H_2O$:THF and 20% $H_2O$:DMSO mixture. At $f_w$ = 90% in both solvents the emission maxima got red shifted to 630 nm (Fig. S8, ESI). We have also carried out pH titration of the **PS-PDI** to determine the compatibility of **PS-PDI** for cellular applications. The optical properties of **PS-PDI** remained stable over a wide pH range of 2.5 to 12 (Fig. S9, ESI). So, probe **PS-PDI** shows good water solubility in mixed organic-aqueous solvent.

### Dynamic light scattering and microscopic studies

To support the aggregation of **PS-PDI** in mixed organic-aqueous solvents, we have also carried out dynamic light scattering (DLS) experiments of **PS-PDI** in THF:$H_2O$ (1:1) and DMSO:$H_2O$ (1:9) solution. The DLS analysis of **PS-PDI** ($1x10^{-5}$ M) in THF:$H_2O$ (1:1) solution revealed the formation of aggregates with diameter in the range of 300-500 nm (Fig. 2a), whereas **PS-PDI** undergoes aggregation in DMSO:$H_2O$ (1:9) to form larger aggregates with diameter in the range of 800-1100 nm (Fig. 2d) and thus truly support the aggregation of **PS-PDI** as observed through photophysical measurements.

To decipher the solvent effect, the self-assembly of **PS-PDI** in THF:$H_2O$ (1:1) and DMSO:$H_2O$ (1:9) have been investigated using microscopic techniques. The scanning electron microscopic (SEM) images of thin film on TLC plate prepared by drop cast technique from solution of **PS-PDI** in THF:$H_2O$ (1:1) shows nanosphere morphology with diameter in the range of 300-500 nm in consonance with DLS experiment (Fig. 2b). We also observe that many of the nanospheres have an open hole on the surface and the diameter of this hole is in the range of 20-25 nm (Fig. 2b, Inset).

The presence of such internal voids represent feature reminiscent of vesicle structure and reason for such voids could be attributed to presence of hydrophilic (water) molecules which help PDI (hydrophobic) part to arrange in vesicle structure. Similarly, transmission electron microscopic (TEM) images further corroborated the nanospherical structure of **PS-PDI** in THF:$H_2O$ (1:1) (Fig. 2c) (Fig. S10, ESI).

On the other hand, the SEM images of thin films of **PS-PDI** deposited from DMSO:$H_2O$ (1:9) solution reveal circular 'Hair-brush' like pattern where small nanorods-like structure are protruding out in 3D fashion with diameter of nanorods in the range of 300-500 nm (Fig. 2e). Very few larger aggregates of size 700 nm were also observed. As shown in figure 2e small nanospheres or rods fused together to form long nanorods whose length extended up to >1 µm and thus results are in consonance with DLS experiments. Similarly, TEM images of **PS-PDI** recorded in DMSO:$H_2O$ (1:9) reveal rod-like assembly on the Cu grid (Fig. 2f). The presence of few diffraction spots in the selected area electron diffraction (SAED) pattern in high resolution TEM (HRTEM) confirmed partial crystalline nature of rod-like assembly (Fig. 2f, Inset) (Fig. S11, ESI).

We anticipate that **PS-PDI** in the presence of $Pd^0$, would undergo depropargylation to produce PDI-OH (PDI-$O^-Na^+$) species and thus would result in segregation of PDI molecule from aggregated structure due to electrostatic repulsions. So, the mechanism or interaction of **PS-PDI** with $Pd^0$ was also explored with DLS experiments. From particle size analysis, we observed that the size of the **PS-PDI** aggregate decreases to <10 nm on interaction with $Pd^0$ in both THF:$H_2O$ (1:1) (Fig. 3a) and DMSO:$H_2O$ (1:9) (Fig. 3d) mixtures.

The micrographs of **PS-PDI**+$Pd^0$ mixture in THF:$H_2O$ (1:1) shows decrease in the size of the nanosphere (Fig. 3b,c) with average diameter in the range of 100-200 nm, with minimum size of 70 nm which we have found on the SEM and TEM data.

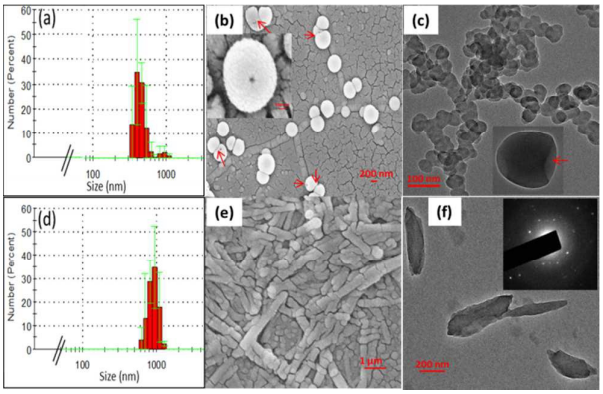


**Fig. 2** (a) DLS analysis of **PS-PDI** ($1x10^{-5}$ M) in THF:$H_2O$ (1:1) solution; (b/c) SEM/TEM images for self-assembled nanospheres of **PS-PDI** ($1x10^{-5}$ M in THF:$H_2O$, 1:1); arrows in image b indicate the presence of open hole on the surface of nanosphere (Inset b/c: image of single nanosphere); (d) DLS analysis of **PS-PDI** ($1x10^{-5}$ M) in DMSO:$H_2O$ (1:9) solution; (e/f) SEM/TEM images for self-assembled nanorods of **PS-PDI** ($1x10^{-5}$ M) in DMSO:$H_2O$, (1:9).

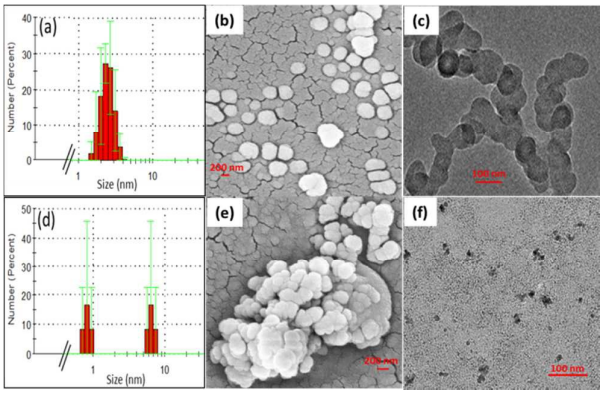


**Fig. 3** (a) DLS analysis of **PS-PDI** ($1x10^{-5}$ M) upon the addition of $Pd^0$ in THF:$H_2O$ (1:1) solution; (b/c) SEM/TEM images of morphological changes in self-assembled **PS-PDI** on addition of $Pd^0$ in THF:$H_2O$ (1:1) solution; (d) DLS analysis of **PS-PDI** ($1x10^{-5}$ M) upon the addition of $Pd^0$ in DMSO:$H_2O$ (1:9) solution; (e/f) SEM/TEM images of morphological changes in self-assembled **PS-PDI** on addition of $Pd^0$ in DMSO:$H_2O$ (1:9) solution.

View Article Online
DOI: 10.1039/C6TB00512H





We also observed complete loss of nanorods assembly with addition of $Pd^0$ in DMSO:$H_2O$ (1:9) and instead we observed formation of smaller size spherical aggregates with diameter of <200 nm (Fig. 3e). Similarly, in the TEM data, we have found that size of the nanosphere/rods dramatically reduces in DMSO:$H_2O$ (1:9) (Fig. 3f) in consonance with DLS studies. Moreover, the nanospheres of **PS-PDI** itself and spherical structure observed for **PS-PDI**+$Pd^0$ mixture in both THF:$H_2O$ (1:1) and DMSO:$H_2O$ (1:9) show amorphous nature because no diffraction pattern was observed in SAED recorded in HRTEM (Fig. S12-13, ESI).

**Palladium detection with PS-PDI aggregates**

The absorption spectrum of **PS-PDI** (c = $1x10^{-5}$ M) in HEPES buffer-THF (1:1, v/v, pH 7.3) solution, where it exist in partial aggregated form, exhibits maxima at 543 nm and on excitation at 490 nm, it shows emission maxima at 564 nm. The UV-Vis titration of **PS-PDI** on addition of $Pd(PPh_3)_4$, as a source of $Pd^0$, showed gradual decrease in the absorbance at 543 nm with concomitant appearance of new band in the NIR region at 710 nm due to ICT process and then attained plateau after reaching its limiting value at $3x10^{-5}$ M concentration of $Pd^0$ (Fig. 4a). The ratiometric plot of $A_{710}/A_{543}$ vs $Pd^0$ concentration shows two linear increases between $10^{-6}$ - $9x10^{-6}$ M and $9x10^{-6}$ – $2x10^{-5}$ M of $Pd^0$, followed by non-linear behavior up to $3x10^{-5}$ M. The detection limit of **PS-PDI** for $Pd^0$ was found to be $1.2x10^{-7}$ M (3σ/slope).[38] The visually detectable colour change of the solution of **PS-PDI** from pink to colourless was observed. The isosbestic point was observed at 560 nm.

Similarly, the fluorescent titration of **PS-PDI** shows that on addition of $Pd^0$, the emission band at 564 nm gradually decreases due to PET process and then it achieves the plateau at $4x10^{-5}$ M concentration of $Pd^0$ (Fig. 4b). In this process, the fluorescence quantum yield[39] decreased from 0.8 (for **PS-PDI**) to 0.26 (**PS-PDI**+$Pd^0$ mixture). The Stern-Volmer plot follows the linear relation between the concentration ranges of $1x10^{-6}$ – $2.5x10^{-5}$ M. The Stern-Volmer constant value ($K_{sv}$) is $1x10^5$ $M^{-1}$. The minimum detection limit of $Pd^0$ was found to be $2.1x10^{-8}$ M (3σ/slope) (Fig. 4b, Inset).

The absorption spectrum of **PS-PDI** in HEPES buffer:DMSO (9:1 v/v, pH 7.3), where it exist in highly aggregated form, shows $\lambda_{max}$ at 510 nm. On gradual addition of $Pd^0$ solution to the solution of **PS-PDI** (c = $1x10^{-5}$ M), we observed that **PS-PDI** produce a new broad band with $\lambda_{max}$ at 700 nm, attributed to the ICT, which attained a plateau at $3x10^{-5}$ M concentration of $Pd^0$ (Fig. S14, ESI). Similarly, weak fluorescence of **PS-PDI** in HEPES buffer:DMSO (9:1 v/v, pH 7.3) solution at 630 nm undergoes fluorescence quenching on addition of $Pd^0$ and attained a plateau at $3x10^{-5}$ M concentration of $Pd^0$ (Fig. S15, ESI). The detection limit of **PS-PDI** for $Pd^0$ was found to be $6.6x10^{-9}$ M (3σ/slope), which is ~30 times lower in comparison to THF:$H_2O$ (1:1). **PS-PDI**, shows visible colour change from

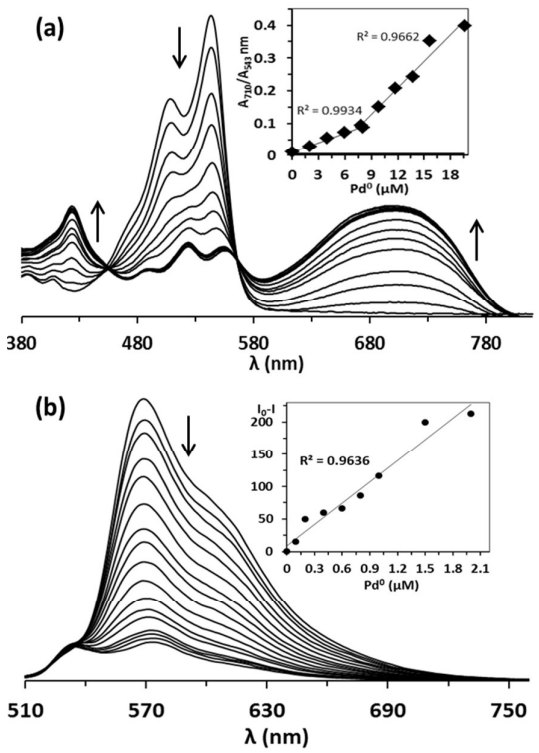


**Fig. 4** (a) UV-Vis absorption, (b) fluorescence spectra of **PS-PDI** ($1x10^{-5}$ M) after incremental addition of $Pd^0$ recorded in HEPES buffer-THF (1:1, v/v, pH 7.3); Inset (a): ratiometric plot of $A_{710}/A_{543}$ vs conc. of $Pd^0$; Inset (b): calibration curve for determining the lowest limit of detection; All spectra were recorded after time interval of 1 hour.

purple to light brown on addition of $Pd^0$ ($3x10^{-5}$ M). All these spectroscopic changes in **PS-PDI** (c = $1x10^{-5}$ M, HEPES buffer:DMSO (9:1, v/v) were observed within a couple of minutes of addition of $Pd^0$ (direct titration) in comparison to one hour time interval in HEPES buffer:THF (1:1, v/v) solvent system. The increase in sensitivity and fast response of **PS-PDI** in DMSO:$H_2O$ (1:9, v/v) can be attributed to aggregation because as the $Pd^0$ interact with aggregates of **PS-PDI**, $Pd^0$ finds several **PS-PDI** molecules in its close vicinity in comparison to interaction of $Pd^0$ with **PS-PDI** in molecularly dissolved state. Interestingly, the optical properties of **PS-PDI** in the presence of other metal ions such as $Zn^{2+}$, $Ni^{2+}$, $Hg^{2+}$, $Li^+$, $K^+$, $Cs^+$, $Ba^{2+}$, $Co^{2+}$, $Ca^{2+}$, $Mg^{2+}$, $Pb^{2+}$, $Sr^{2+}$, $Fe^{2+}$, $Cu^{2+}$, $Pd^{2+}$ ($1x10^{-3}$ M) remained unchanged.

We have also carried out optical titration of **DPS-PDI** (c = $1x10^{-5}$ M) in the presence of $Pd^0$. On gradual addition of $Pd^0$, **DPS-PDI** (HEPES buffer-THF, 1:1, v/v, pH 7.3) showed gradual decrease in the absorbance at 550 nm with concomitant appearance of new band at 630 nm and then attained plateau after reaching its limiting value at $2x10^{-5}$ M concentration of $Pd^0$. We also observed that absorbance intensity at 550 nm shows only 25% decrease in comparison to 80% decrease in

View Article Online
DOI: 10.1039/C6TB00512H




case of **PS-PDI**. Visually detectable colour change of the solution of **DPS-PDI** from pink to violet, on addition of $Pd^0$ was observed. On the other hand, the emission band of **DPS-PDI** at 580 nm gradually decreases as the concentration of $Pd^0$ is increased and then it achieves the plateau at $2x10^{-5}$ M concentration of $Pd^0$ (Fig. S16, ESI)

### Imaging of $Pd^0$ in Hela Cells using PS-PDI aggregates

Before performing the cell imaging studies, cytotoxicity of **PS-PDI** on HeLa cells using 3-(4,5-dimethyl-2-thiazolyl)-2,5-diphenyl-2H-tetrazolium bromide (MTT) assay was checked. Very low cytotoxic effect on the proliferation of the HeLa cells was observed in the presence of different concentrations such as $5x10^{-6}$ M, $1x10^{-5}$ M and $2x10^{-5}$ M of **PS-PDI** (cell viability 92.6%, 90.5% and 88% respectively) (Fig. S17, ESI). These data indicates that **PS-PDI** (c = $1x10^{-5}$ M) can be considered to have low cytotoxicity to HeLa cells and did not significantly affect the cell viability.

To test the cell-internalization ability of **PS-PDI** and its response towards $Pd^0$, HeLa cells were used. Brightfield image showed that the HeLa cells were healthy and viable throughout the experiment (Fig. 5a). HeLa cells, themselves (without **PS-PDI**) and after incubation with $Pd^0$ ($4x10^{-5}$ M), did not exhibit any fluorescence (Fig. 5b-c). However, when HeLa cells were imaged after incubation with **PS-PDI** for 30 min at 37°C, it showed bright red fluorescence in the cytoplasmic region ($\lambda_{ex}$ = 488) (Fig. 5d). This depicted that **PS-PDI** is permeable to HeLa cells and can be used for bioimaging of $Pd^0$ in the live cells.

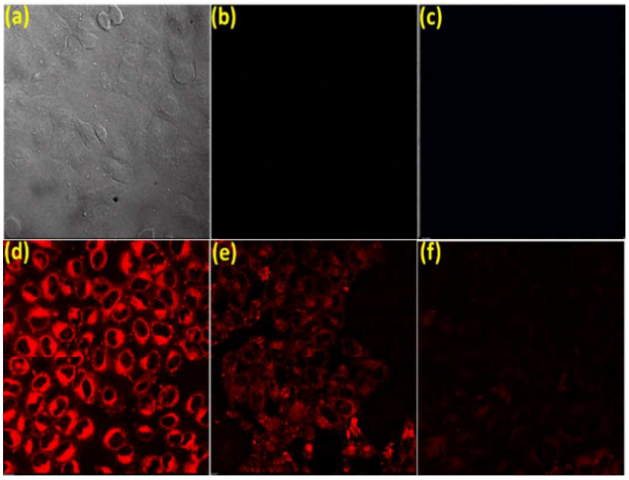


**Fig. 5** Confocal microscopic images of HeLa cells: (a) brightfield image of HeLa cells (b) fluorescence image of HeLa cells without **PS-PDI**; (c) fluorescence image of HeLa cells incubated with $Pd^0$ ($4x10^{-5}$ M) for 4 hours; (d) fluorescence image of HeLa cells incubated with **PS-PDI** ($1x10^{-5}$ M) for 30 min; (e) fluorescence image of HeLa cells incubated with **PS-PDI** ($1x10^{-5}$ M) for 30 min followed by incubation with $Pd^0$ ($2x10^{-5}$ M) for four hours and (f) fluorescence image of HeLa cells incubated with **PS-PDI** ($1x10^{-5}$ M) for 30 min and then incubated with $Pd^0$ ($4x10^{-5}$ M) for four hours. The fluorescence images were acquired using excitation at 488 nm.

Then **PS-PDI** treated ($1x10^{-5}$ M for 30 min) HeLa cells were washed with PBS buffer (pH = 7.4, 2 times) supplemented with 10% DMSO. Subsequently, $1x10^{-5}$ M, $2x10^{-5}$ M, $3x10^{-5}$ M and $4x10^{-5}$ M $Pd^0$ was added and HeLa cells were further incubated for 4h at 37°C before imaging. We observed that fluorescence intensity of **PS-PDI** inside the HeLa cells was significantly quenched in a concentration dependent manner and, intracellular fluorescence intensity vanished almost completely at $4x10^{-5}$ M concentration of **PS-PDI** (Fig. 5e-f).

### Kinetic Profile of PS-PDI aggregates

The investigation of time dependent and concentration dependent kinetic profiles of **PS-PDI** revealed rapid response to $Pd^0$ with good correlation. For kinetic experiments the absorption and emission spectrum of **PS-PDI** in presence of different concentrations of $Pd^0$ were recorded after regular time intervals in DMSO:$H_2O$ (1:9) and THF:$H_2O$ (1:1). Impressively, **PS-PDI** (c = $1x10^{-5}$ M) in DMSO:$H_2O$ (1:9), where it exists in aggregated state, when treated with $5x10^{-6}$ M concentration of $Pd^0$, we observed that within 11 min of response time, the emission intensity at 630 nm reached its limiting value. The rate constant[40] for Pd triggered depropargylation reaction of **PS-PDI** was found to be *K* = slope x 2.303 = 0.16 $s^{-1}$. Moreover, **PS-PDI** required only 7 and 4 min for depropargylation in the presence of $1x10^{-5}$ M and $2x10^{-5}$ M concentration of $Pd^0$ with rate constant of 0.23 $s^{-1}$ and 0.4 $s^{-1}$, respectively. On the other hand, when **PS-PDI** was treated with $5x10^{-6}$ M and $2x10^{-5}$ M concentration of $Pd^0$, the absorbance at 700 nm increased and reached its limiting value within 16 min (K = 0.15 $s^{-1}$) and 12 min (0.21 $s^{-1}$), respectively (Fig. S18-19, ESI).

**PS-PDI** (c = $1x10^{-5}$ M) in THF:$H_2O$ (1:1) when treated with $8x10^{-5}$ M concentration of $Pd^0$, we observed that the emission at 564 nm dramatically decreased and reached its limiting value within 6 min (Figure 6b). The rate constant calculated from the plot of emission at 564 nm versus time found to be 0.148 $s^{-1}$ within first 0-3 min and then rate slows down in the next 3-6 min (0.036 $s^{-1}$) before it achieves the plateau. The depropargylation reaction of **PS-PDI** with $6x10^{-5}$ M and $4x10^{-5}$ M concentration of $Pd^0$ completed in 10 min and 16 min, respectively with rate constant value found to be 0.143 $s^{-1}$ and 0.06 $s^{-1}$. Similarly, **PS-PDI** when treated with $8x10^{-5}$ M concentration of $Pd^0$, we observed that within 10 min of response time, the absorbance at 710 nm dramatically increased to its limiting value (Fig. 6a). The rate constant was found to be *K* = slope x 2.303 = 0.136 $s^{-1}$. We also observed that **PS-PDI** required 24 min (K = 0.03 $s^{-1}$) and 60 min (K = 0.027 $s^{-1}$) for completion of depropargylation reaction at $6x10^{-5}$ M and $4x10^{-5}$ M concentrations of $Pd^0$, respectively (Fig. 6a-b Inset and Fig. S20-21, ESI). From these kinetic profiles, we conclude that **PS-PDI** responds to $Pd^0$ much faster (~5-8 times) when present in aggregated form in comparison to their molecularly dissolved form.

View Article Online
DOI: 10.1039/C6TB00512H





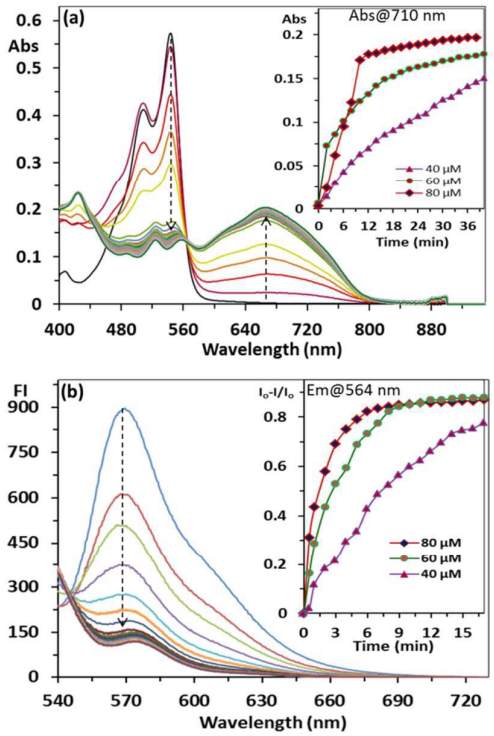


**Fig. 6** (a) UV-Vis absorption (b) emission spectra of **PS-PDI** ($1x10^{-5}$ M) after addition of $Pd^0$ ($8x10^{-5}$ M) in HEPES buffer-THF (1:1, v/v, pH 7.3) recorded after every 2 minutes for absorption and 1 minute for emission; Time dependent and concentration dependent kinetic profiles for **PS-PDI** ($1x10^{-5}$ M) at $\lambda_{abs}$ = 710 nm (Inset a) and at $\lambda_{em}$ = 564 nm (Inset b) after addition of $4x10^{-5}$ M, $6x10^{-5}$ M and $8x10^{-5}$ M of $Pd^0$ recorded in HEPES buffer-THF (1:1, v/v, pH 7.3).

### PS-PDI aggregates as general Pd sensor

$Pd^{2+}$ is generally known to be the most toxic metal ion among $Pd^0$, $Pd^{2+}$ and $Pd^{4+}$ ions that exist under physiological conditions. Since $Pd^{2+}$ can be easily reduced to $Pd^0$, our **PS-PDI** could be utilized for sensing of $Pd^{2+}$ in the presence of $NaBH_4$-$PPh_3$ conditions. The UV-Vis spectrum of **PS-PDI** in HEPES buffer-THF (1:1 v/v, pH 7.3), or HEPES buffer-DMSO (9:1 v/v, pH 7.3) and $NaBH_4$-$PPh_3$ (350 μL each of 10 mM solution) on gradual addition of $PdCl_2$, showed gradual decrease in the absorption band at 543 nm with concomitant appearance of new red shifted band at 710 nm with isosbestic point at 560 nm. The ratiometric behaviour ($A_{710}/A_{543}$) of **PS-PDI** shows good correlation up to $2x10^{-5}$ M $Pd^{2+}$ ions. Similarly, the fluorescence spectrum of **PS-PDI** underwent fluorescence quenching in the presence of $Pd^{2+}$ at 564 nm (Fig. S22, ESI). We also performed UV-Vis experiments of **PS-PDI** (c = $1x10^{-5}$ M) in the presence of $2x10^{-5}$ M $Pd^0$ or $Pd^{2+}$ (with or without $NaBH_4$-$PPh_3$) and observed that both samples exhibit similar intensity for 710 nm absorption band whereas $Pd^{2+}$ without $NaBH_4$-$PPh_3$ did not convert **PS-PDI** to **PDI-OH** and thus support our hypothesis for application of **PS-PDI** as general Pd sensor system (Fig. 7a).

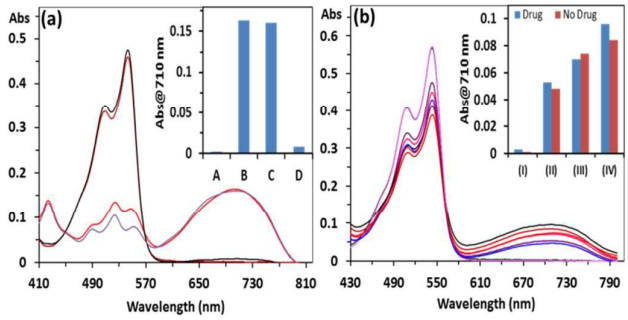


**Fig. 7** (a) UV-Vis absorption spectra of **PS-PDI** in the presence of $Pd^0$ and $Pd^{2+}$ showing applicability of **PS-PDI** as general Pd sensor system; (Inset) Bar graph showing A = **PS-PDI**, B = **PS-PDI** +$Pd^0$, C = **PS-PDI** +$Pd^{2+}$+$NaBH_4$-$PPh_3$, D = **PS-PDI** +$Pd^{2+}$; (b) UV-Vis absorption spectra of **PS-PDI** with $Pd^0$ in the presence and absence of drug; (Inset) Bar graph showing (I) = **PS-PDI**, (II) = **PS-PDI** +$Pd^0$ ($4x10^{-5}$ M), (III) = **PS-PDI** + $Pd^0$ ($6x10^{-5}$ M), (IV) = **PS-PDI** + $Pd^0$ ($1x10^{-5}$ M).

### Application of PS-PDI aggregates for Analysis of Pd in pharmaceutical, environmental and urine samples

To check the suitability of our **PS-PDI** for sensing of $Pd^0$ in the pharmaceutical drug, we prepared various samples of **PS-PDI** that contained different concentrations of $Pd^0$ with and without drug (disprin tablet) in HEPES buffer-THF (1:1, v/v) (pH 7.3). Interestingly, we observed that the absorption intensity of **PS-PDI** solution at respective concentrations of $Pd^0$ (0, $4x10^{-6}$, $6x10^{-6}$ and $1x10^{-5}$ M) at 710 nm were nearly same (<10%) in the absence and presence of drug (Fig. 7b) and thus demonstrate the utility of **PS-PDI** for determining the $Pd^0$ in pharmaceutical sample.

**PS-PDI** could also be used for detection of unknown concentration of $Pd^{2+}$ in human urine sample using calibration curve. To a solution of **PS-PDI** ($1x10^{-5}$ M) in HEPES buffer-THF (1:1, v/v, pH = 7.3), 350 μL each of $NaBH_4$ and $PPh_3$ was added followed by addition of 100 μL of urine sample (1 mL urine diluted to 100 mL with $H_2O$) in separate flask. The $Pd^{2+}$ concentration in adult urine sample was found to be 0.18 μg/l (Fig. 8).

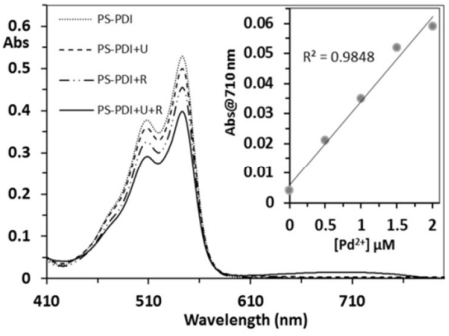


**Fig. 8** UV-Vis absorption spectrum of **PS-PDI** ($1x10^{-5}$ M) and **PS-PDI** + urine showing the capability of **PS-PDI** for sensing of $Pd^{2+}$ in urine sample; U = urine sample; R = reducing agent ($NaBH_4$-$PPh_3$); Inset: calibration curve for determining the unknown concentration of $Pd^{2+}$ in urine sample.

View Article Online
DOI: 10.1039/C6TB00512H




We also carried out analysis of $Pd^0$ in complicated environmental samples such as tap water, pond water and industrial waste water collected from different sources. The different samples were spiked with various concentrations of $Pd^0$ ions. The concentration thus, determined by absorbance spectroscopy agreed with actual concentration with a relative error of 1.9% or better and a RSD below 3.9% (tap water); relative error of 1.2% or better and a RSD below 2.0% or better (pond water) and relative error of 1.7% or better and a RSD below 4.3% or better (industrial waste water) (Table 1). Moreover, The concentration thus, determined by fluorescence spectroscopy agree with actual concentration with a relative error of 1.3% or better and a RSD below 2.7% (tap water); relative error of 2.3% or better and a RSD below 2.6% or better (pond water) and relative error of 0.9% or better and a RSD below 1.8% or better (industrial waste water) (Table 1 and Table S2).

### Chemodosimeter mechanism

The cause of change in colour or fluorescence intensity of the solution of **PS-PDI** on addition of $Pd^0$ could be attributed to de-propargylation to provide **PDI-OH** parallel to the earlier reported literature (scheme 3).[41] For proving this mechanism, PDI-OH was synthesized by earlier reported procedure[42] and its UV-Vis spectrum was recorded in HEPES buffer-THF (1:1, v/v, pH 7.3). It exhibits two absorption maxima at 543 and 710 nm and a weak fluorescence at 564 nm in the emission spectrum. In the pH titration of **PDI-OH** in THF:$H_2O$ (1:1, v/v) we observed decrease in the intensity of absorption band at 543 nm whereas absorption intensity increased at 710 nm with change in the pH of the solution from 6.0 to 11.0 (Fig. S23, ESI).

**Table 1**. Application of **PS-PDI** for the determination of $Pd^0$ in the various environmental samples (tap water, pond water and industrial waste water)

| Sample | Added (μM) | Conc. ± SD[a] (μM) / (relative error) **(UV @710 nm)** | Added (μM) | Conc. ± SD[a] (μM) / (relative error) **(FI @564 nm)** |
|---|---|---|---|---|
| Tap Water | 5.0 | 5.0 ± 0.08 (1.10) | 10.0 | 10.0 ± 0.04 (0.31) |
| | 10.0 | 10.0 ± 0.19 (1.31) | 15.0 | 15.0 ± 0.05 (0.26) |
| | 25.0 | 25.0 ± 0.55 (1.55) | 20.0 | 20.0 ± 0.24 (0.69) |
| Pond Water | 15.0 | 15.0 ± 0.12 (0.53) | 5.0 | 5.0 ± 0.01 (0.19) |
| | 20.0 | 20.0 ± 0.15 (0.58) | 15.0 | 15.0 ± 0.27 (1.37) |
| | 25.0 | 25.0 ± 0.23 (0.70) | 25.0 | 25.0 ± 0.33 (1.02) |
| Industrial Waste water | 5.0 | 5.0 ± 0.12 (1.64) | 5.0 | 5.0 ± 0.05 (0.66) |
| | 10.0 | 10.0 ± 0.11 (0.77) | 15.0 | 15.0 ± 0.11 (0.38) |
| | 25.0 | 25.0 ± 0.76 (2.17) | 20.0 | 20.0 ± 0.06 (0.16) |

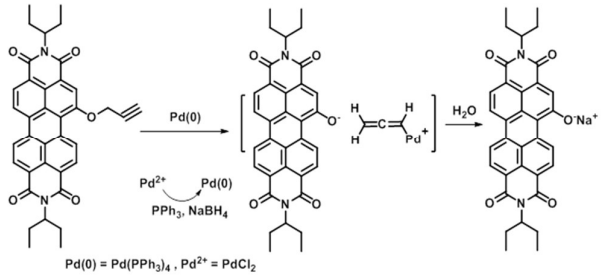


**Scheme 3**. The proposed mechanism for the depropargylation reaction of **PS-PDI** in the presence of $Pd^0$ and $Pd^{2+}$ (with reducing agents).

### Competitive experiments

To ascertain the selectivity of **PS-PDI** for $Pd^0$, the UV-Vis and emission spectrum of **PS-PDI** were also recorded in the presence of other probable interfering metal ions. We observed that only addition of $Pd^0$ results in increase of absorbance at 710 nm whereas, on addition of other metal ions no change in the absorption spectrum was observed. Similarly, the fluorescence intensity of **PS-PDI** at 564 nm got quenched on addition of $Pd^0$, whereas no significant quenching of fluorescence intensity was observed in the presence of other metal ions. Moreover, solutions of **PS-PDI** ($1x10^{-5}$ M), one of the probable interfering metal ions ($1x10^{-4}$ M) and $Pd^0$ ($2x10^{-5}$ M) were prepared and their absorption and emission spectra were recorded. The absorption and emission intensity of **PS-PDI**-$Pd^0$ mixture and **PS-PDI**-$Pd^0$-$M^{n+}$ solution remained unperturbed and thus points out that presence of other probable interfering metal ions does not interfere in the detection of $Pd^0$ (Fig. S24, ESI).

## Conclusion

**PS-PDI** shows aggregation in mixed organic-aqueous solvents with formation of self-assembled nanovesicles in THF:$H_2O$ (1:1) and nanorod-like structures in DMSO:$H_2O$ (1:9) as evidenced by DLS, SEM and TEM studies. The aggregates of **PS-PDI** respond to $Pd^0$ via de-aggregation or dis-assembly of nanovesicles/rods morphology. In solution form, **PS-PDI** aggregates gives new red-shifted absorption maxima in the NIR region at 710 nm (ratiometric) and quenching of its emission intensity at 630 nm or 564 nm in the presence of $Pd^0$ and $Pd^{2+}$ (with reducing reagents) in aqueous buffer and could be useful as general $Pd^0$/$Pd^{2+}$ chemodosimeter. $Pd^0$ mediated depropargylation of the **PS-PDI** to the PDI-OH has been assigned as the cause of observed photophysical changes in the presence of $Pd^0$. **PS-PDI** was successfully applied for the detection of $Pd^0$ in environmental and drug samples and $Pd^{2+}$ in urine sample. Moreover, **PS-PDI** could be easily internalized into HeLa cells with low cytotoxicity and could detect $2x10^{-5}$ – $4x10^{-5}$ M of $Pd^0$ in live HeLa cells.

View Article Online
DOI: 10.1039/C6TB00512H




## Acknowledgements

This work was supported by the CSIR (02(0084)/12/EMR-II) and DST-SERB fast track grant (CS/2012/088). We thank UGC for CAS status to the department, UPE programme and DST for FIST programme. LSM and KK are thankful to UGC for SRF and DST-SERB for JRF fellowship, respectively. Live cell experiments were supported by a grant from DBT, India (BT/IN/German /13/VK/2010) to VV.

## Notes and references

1. a) F. Wurthner, *Chem. Commun.* **2004**, 1564-1579; b) F. Wurthner, C. R. Saha-Moller, B. Fimmel, S. Ogi, P. Leowanawat, D. Schmidt, *Chem. Rev.*, **2015,** 115, 11967-11998; c) H. Langhals, *Heterocycles* **1995**, *40*, 477-500.
2. a) C. Huang, S. Barlow, S. R. Marder, *J. Org. Chem.* **2011**, *76*, 2386-2407; b) X. Guo, A. Facchetti, T. J. Marks, *Chem. Rev.* **2014**, *114*, 8943-9021
3. a) C. Li, H. Wonneberger, *Adv. Mater.* **2012**, *24*, 613-636; b) X. W. Zhan, A. Facchetti, S. Barlow, T. J. Marks, M. A. Ratner, M. R. Wasielewski, S. R. Marder, *Adv. Mater.* **2011**, *23*, 268-284.
4. a) Q. L. Zhao, S. Zhang, Y. Liu, J. Mei, S. J. Chen, P. Lu, A. J. Qin, Y. G. Ma, J. Z. Sun, B. Z. Tang, *J. Mater. Chem.* **2012**, *22*, 7387-7394; b) R. C. Liu, M. W. Holman, L. Zang, D. M. Adams, *J. Phys. Chem. A* **2003**, *107*, 6522-6526.
5. A. Wicklein, S. Ghosh, M. Sommer, F. Wurthner, M. Thelakkat, *ACS Nano* **2009**, 3, 1107-1114.
6. a) Y. Li, T. Liu, H. Liu, M.Z. Tian, Y. Li, *Acc. Chem. Res.* **2014**, *47*, 1186-1198; b) W. Herbst, K. Hunger, *Industrial Organic Pigments,* VCH -Weinheim, (3rd Ed.) **2004**.
7. a) H. Langhals, *Helv. Chim. Acta* **2005**, *88*, 1309-1343; b) M. J. Ahrens, *Chem. Mater.* **2003**, *15*, 2684-2686.
8. a) J. E. Anthony, *Chem. Mater.* **2011**, *23*, 583-590; b) A. Ringk, X. R. Li, F. Gholamrezaie, E. C. P Smits, A. Neuhold, Moser, C. V. D. Marel, G. H. Gelinck, R. Resel, D. M. D. Leeuw, P. Strohriegl, *Adv. Funct. Mater.* **2013**, *23*, 2016-2023.
9. M. Thelakkat, P. Posch, H.-W. Schmidt, *Macromolecules* **2001**, *34*, 7441-7447.
10. a) P. Singh, K. Kumar, G. Bhargava, S. Kumar, *J. Mater. Chem. C*, **2016**, *4*, 2488-2497; (b) P. Singh, L. S. Mittal, V. Vanita, R. Kumar, G. Bhargava, A. Walia, S. Kumar, *Chem. Commun.* **2014**, *50*, 13994-13997; c) P. Singh, L. S. Mittal, S. Kumar, G. Bhargava, S. Kumar, *J. Fluoresc.* **2014**, 909-915; d) M. Marcia, P. Singh, F. Hauke, M. Maggini, A. Hirsch, *Org. Biomol. Chem.* **2014**, *12*, 7045-7058.
11. a) A. Weißenstein, F. Wurthner, *Chem. Commun.* **2015**, *51*, 3415-3418; b) T. H. Rehm, M. R. Stojkovic, S. Rehm, M. Skugor, I. Piantanida, F. Wurthner, *Chem. Sci.* **2012**, *3*, 3393-3397.
12. a) P. D. Frischmann, V. Kunz, V. Stepanenko, F. Wurthner, *Chem. – Eur. J.* **2015**, *21*, 2766-2769; b) S. Malkondu, S. Erdemir, *Dyes Pigm.,* **2015**, *113*, 763-769.
13. a) M. A. Kaloo, R. Mishra, J. Sankar, *J. Mater. Chem. C* **2015**, *3*, 1640-1644; b) H.-R. Cheng, Y. Qian, *Sensors Actuators Chem. B* **2015**, *219*, 57-64.
14. a) B. Roy, T. Noguchi, D. Yoshihara, Y. Tsuchiya, A. Dawn, S. Shinkai, *Org. Biomol. Chem.* **2014**, *12*, 561-565; b) Y. Wang, L. Zhang, G. Zhang, Y. Wu, S. Wu, J. Yu, L. Wang, *Tetrahedron Lett.* **2014**, *55*, 3218-3222.
15. a) K. Liu, Z. Xu, M. Yin, W. Yang, B. He, W. Wei, J. J. Shen, *J. Mater. Chem. B* **2014**, *2*, 2093-2096; b) A. K. Dwivedi, M. Pandeeswar, T. Govindaraju, *ACS Appl. Mater. Interfaces* **2014**, *6*, 21369-21379.
16. J. Li, Y. Wu, F. Song, G. Wei, Y. Cheng, C. J. Zhu, *J. Mater. Chem.* **2012**, *22* , 478-482.
17. L. Zhang, Y. Wang, J. Yu, G. Zhang, X. Cai, Y. Wu, L. Wang, *Tetrahedron Lett.* **2013**, *54*, 4019-4022.
18. a) X. Feng, Y. An, Z. Yao, C. Li, G. Shi, *ACS Appl. Mater. Interfaces* **2012,** *4*, 614-618; b) B. Wang, F. Wang, H. Jiao, X. Yang C. Yu, *Analyst* **2010**, *135*, 1986-1991.
19. a) X. Lu, W. Zhu, Y. Xie, X. Li, Y. Gao, F. Li, H. Tian, H., *Chem. Eur. J.* **2010**, *16*, 8355-8364; b) J. Ren, X.L. Zhao, Q.C. Wang, C.F. Ku, D.H. Qu, C.P. Chang, H. Tian, *Dyes Pigm.* **2005**, *64*, 193-200.
20. X. He, H. Liu, Y. Li, S. Wang, Y. Li, N. Wang, J. Xiao, X. Xu, D. Zhu, *Adv Mater.* **2005**, *17*, 2811-2815.
21. a) L. Chunli, Z. Haiyan, L. Xiaotian, Z. Weiguang, H. Yongwei, *J. Mater.Chem.C* **2015, 3,** 2778-2782; (b) H. Yongwei, Z. Weiguang, Z. Haiyan, L. Chunli, *J. Mater. Chem. C* **2015**, *3*, 466-472.
22. C. Backes, C. D. Schmidt, F. Hauke, C. Bottcher, *J. Am. Chem. Soc.* **2009**, *131*, 2172-2184.
23. a) L. Zhang, Y. K. Che, J. S. Moore, *Acc. Chem. Res.* **2008**, *41*, 1596-1608; b) D. Gorl, X. Zhang, F. Wurthner, *Angew. Chem., Int. Ed.* **2012**, *51*, 6328-6348.
24. a) Z. J. Chen, V. Stepanenko, V. Dehm, P. Prins, L. D. A. Siebbeles, J. Seibt, P. Marquetand, V. Engel, F. Wurthner, *Chem. –Eur. J.* **2007**, *13*, 436-449; b) F. Fennel, S. Wolter, Z. Q. Xie, P. A. Plotz, O. Kuhn, F. Wurthner, S. Lochbrunner, *J. Am. Soc. Chem.* **2013**, *135*, 18722-18725; c) M. A. Muth, G. Gupta, A. Wicklein, M. C. Orozco, T. T. Albrecht, M. Thelakkat, *J. Phys. Chem. C* **2014**, *118*, 92-102.
25. a) Y. Sun, C. He, K. Sun, Y. Li, H. L. Dong, Z. H. Wang, Z. B. Li, *Langmuir* **2011**, *27*, 11364-11371; b) W. Su, Y. X. Zhang, C. T. Zhao, X. Y. Li, J. Z. Jiang, *ChemPhysChem* **2007**, *8*, 1857-1862; c) X. Q. Li, X. Zhang, S. Ghosh, F. Wurthner, *Chem.-Eur. J.* **2008**, *14*, 8074-8078.
26. a) Z. G. Zhang, C. L. Zhan, X. Zhang, S. L. Zhang, J. H. Huang, A. D. Q. Li, J, N, Yao, *Chem.-Eur. J.* **2012**, *18*, 12305-12313; b) J. Zhou, L. Xue, Y. Shi, X. Y. Li, Q. B. Xue, S. Q. Wang, *Langmuir*, **2012**, *28*, 14386-14394; c) Y. W. Huang, L. N. Fu, W. J. Zou, F. L. Zhang, Z. X. Wei, *J. Phys. Chem. C* **2011**, *115*, 10399-10404.
27. a) S. Sandhu, R. Kumar, P. Singh, A. Mahajan, M. Kaur, S. Kumar, *ACS Appl. Mater. Interfaces* **2015**, *7*, 10491-10500; b) S. Kumar, P. Singh, A. Mahajan, S. Kumar, *Org. Lett.* **2013**, *15*, 3400-3403;
28. a) K. B Joshi, P. Singh, *Tetrahedron Lett.* **2014**, *55*, 3534-3537; b) K. B. Joshi, P. Singh, S. Verma, *Biofabrication* **2009**, *1*, 025002-025007.



 

View Article Online
DOI: 10.1039/C6TB00512H


29. a) P. Singh, V. Venkatesh, J. Kumar, N. Nagapradeep, S. Verma, A. Bianco, *Nanoscale* **2012**, *4*, 1972-1974; b) P. Singh, F. M. Toma, J. Kumar, V. Venkatesh, J. Raya, M. Prato, S. Verma, A. Bianco, *Chem. -Eur. J.* **2011**, *17*, 6772–6780; c) P. Singh, J. Kumar, F.M. Toma, J. Raya, M. Prato, B. Fabre, S. Verma, A. Bianco, *J. Am. Chem. Soc.* **2009**, *131*, 13555–13562.
30. a) S. Cacchi, G. Fabrizi, *Chem. Rev.* **2005**, *105*, 2873-2920; b) H. F. Sore, R. J. Warren, D. Galloway, D. R. Spring, *Chem. Soc. Rev.* **2012**, *41*, 1845-1866.
31. a) R. M. Yusop, A. Unciti-Broceta, E. M. V. Johansson, R. M. Sanchez-Martin, M. Bradley, *Nat. Chem.* **2011**, *3*, 239-243; b) C. L. S. Wiseman, F. Zereini, *Sci. Total Environ.* **2009**, *407*, 2493-2500; c) F. Zereini, C. Wiseman, W. Puettmann, *Environ. Sci. Technol.* **2007**, *41*, 451-456.
32. a) K. Van Meel, A. Smekens, M. Behets, P. Kazandjian, R. VanGrieken, *Anal. Chem.* **2007**, *79*, 6383-6389; b) C. Locatelli, D. Melucci, G. Torsi, *Anal. Bioanal. Chem.* **2005**, *382*, 1567-1573.
33. a) S. Goswami, D. Sen, N. K. Das, H. K. Fun, C. K. Quah, *Chem. Commun.* **2011**, 9101-9103; b) X. J. Peng, H. L. Li, J. L. Fan, F. L. Song, H. Zhu, J. J. Du, S, G. Sun, *Chem.-Eur. J.* **2010**, *16*, 12349-12356; c) B. Zhu, C. Gao, Y. Zhao, C. Liu, Y. Li, Q. Wei, Z. Ma, B. Du, X. Zhang, *Chem. Commun.* **2011**, *47*, 8656-8658.
34. a) M.Y. Chae, A.W. Czarnik, *J. Am. Chem. Soc.* **1992**, *114*, 9704-9705; b) K. Kaur, R. Saini, A. Kumar, V. Luxami, N. Kaur, P. Singh and S. Kumar, *Coord. Chem. Rev.* **2012**, *256*, 1992-2028.
35. M. P. Tracey, D. Pham, K. Koide, *Chem. Soc. Rev.* **2015**, *44*, 4769-4791.
36. a) A. Rajasingh, R. Cohen, E. Shirman, L. J. W. Shimon, B. Rybtchinski, *J. Org. Chem.* **2007**, *72,* 5973-5979; (b) H. Langhals, O. Krotz, K. Polborn, P. Mayer, *Angew. Chem. Int. Ed.* **2005**, *44*, 2427-2428.
37. a) L. M. Wang, Z. J. Chen, G. Zou, L. Zhang, G. J. Zhang, X. F. Cai, M. S. Teng, *Dyes Pigm.* **2012**, *94*, 410-415; b) X. Kong, J. Gao, T. Ma, M. Wang, A. Zhang, Z. Shi, Yanhong Wei, *Dyes Pigm.* **2012**, *95*, 450-454
38. J. Mokac, A. M. Bond, S. Mitchell, G. Scollary, *Pure Appl. Chem.* **1997**, *69*, 297-328.
39. J. N. Demas, G. A. Grosby, *J. Phys. Chem.* **1971**, *75*, 991-1024.
40. a) L. Yuan, W. Lin, Y. Yang, *Chem. Commun.*, **2011**, *47*, 6275–6277; b) S. Goswami, S. Das, K. Aich, D. Sarkar, T. K. Mondal, *Tetrahedron Lett.*, **2014**, *55*, 2695-2699.
41. a) M. Pal, K. Parasuraman, K. R. Yeleswarapu, *Org. Lett.* **2003**, *5*, 349-352; b) B. Liu, H. Wang, T. Wang, Y. Bao, F. Du, J. Tian, Q. Li, R. Bai, *Chem. Commun.* **2012**, *48*, 2867-2869.
42. Y. Li, H. Zheng, Y. Li, S. Wang, Z. Wu, P. Liu, Z. Gao, H. Liu, D. Zhu, *J. Org. Chem.* **2007**, *72*, 2878-2885.